# Ultrahigh-pressure form of SiO_{2} glass with dense pyrite-type crystalline homology

M. Murakami, S. Kohara, N. Kitamura, J. Akola, H. Inoue, A. Hirata, Y. Hiraoka, Y. Onodera, I. Obayashi, J. Kalikka, N. Hirao, T. Musso, A. S. Foster, Y. Idemoto, O. Sakata, and Y. Ohishi

Phys. Rev. B **99**, 045153 — Published 29 January 2019

DOI: 10.1103/PhysRevB.99.045153

# An ultrahigh-pressure form of $SiO_2$ glass with dense pyrite-type crystalline homology

M. Murakami,[1,2]* S. Kohara,[3-7]* N. Kitamura[8,9], J. Akola[9-11] H. Inoue[12], A. Hirata[13-16], Y. Hiraoka[17,16,4], Y. Onodera[18,4], I. Obayashi[19], J. Kalikka[9], N. Hirao[5], T. Musso[11], A. S. Foster[11, 20], Y. Idemoto[8], O. Sakata[3], Y. Ohishi[5]

[1]Department of Earth Sciences, ETH Zürich, Clausiusstrasse 25, Zürich, Switzerland.
[2]Department of Earth and Planetary Materials Science, Tohoku University, Sendai 980-8578, Japan.
[3]Research Center for Advanced Measurement and Characterization, National Institute for Materials Science (NIMS), 1-1-1 Kouto, Sayo-cho, Sayo-gun, Hyogo 679-5148, Japan
[4]Center for Materials Research by Information Integration, NIMS, 1-2-1 Sengen, Tsukuba, Ibaraki 305-0047, Japan.
[5]Research and Utilization Division, Japan Synchrotron Radiation Research Institute, Sayo, Hyogo 679-5198, Japan.
[6]School of Materials Science, Japan Advanced Institute of Science and Technology, Nomi, Ishikawa, 923-1211, Japan.
[7] PRESTO, Japan Science and Technology Agency, Honcho, Kawaguchi, Saitama 332-0012, Japan.
[8]Department of Pure and Applied Chemistry, Faculty of Science and Technology, Tokyo University of Science, Noda, Chiba 278-8510, Japan.
[9]Department of Physics, Tampere University of Technology, P.O. Box 692, FI-33101 Tampere, Finland.
[10]Department of Physics, Norwegian University of Science and Technology, NO-7481 Trondheim, Norway.
[11]Department of Applied Physics, Aalto University, FI-00076 Aalto, Finland.
[12]Institute of Industrial Science, The University of Tokyo, 4-6-1 Komaba Meguro, Tokyo 153-8505, Japan.
[13]Graduate School of Fundamental Science and Engineering, Waseda University, 3-4-1 Ohkubo, Shinjuku, Tokyo, 169-8555, Japan
[14]Kagami Memorial Research Institute for Materials Science and Technology, Waseda University, 2-8-26 Nishiwaseda, Shinjuku, Tokyo, 169-0051, Japan
[15]Mathematics for Advanced Materials-OIL, AIST-Tohoku University, Sendai 980-8577, Japan.
[16]WPI Advanced Institute for Materials Research, Tohoku University, 2-1-1 Katahira, Aoba-ku, Sendai 980-8577, Japan
[17]Kyoto University Institute for Advanced Study, Kyoto University, Yoshida Ushinomiya-cho, Sakyo-ku, Kyoto, 606-8501, Japan
[18]Institute for Integration Radiation and Nuclear Science, Kyoto University, 2-1010 Asashiro-nishi, Kumatori-cho, Sennan-gun, Osaka 590-0494, Japan.
[19]Center for Advanced Intelligence Project, RIKEN, 1-4-1 Nihonbashi, Chuo-ku, Tokyo, 103-0027, Japan
[20]Division of Electrical Engineering and Computer Science, Kanazawa University, Kanazawa 920-1192, Japan.

*Corresponding authors: Motohiko Murakami (motohiko.murakami@erdw.ethz.ch), Shinji Kohara (kohara.shinji@nims.go.jp).

**Abstract**

**High-pressure synthesis of denser glass has been a long-standing interest in condensed matter physics and materials science because of its potentially broad industrial application. Nevertheless, understanding its nature under extreme pressures has yet to be clarified due to experimental and theoretical challenges. Here we revealed the novel formation of $OSi_4$ tetraclusters associated with that of $SiO_7$ polyhedra in $SiO_2$ glass under ultrahigh pressures to 200 gigapascal confirmed both experimentally and theoretically. Persistent homology analyses with molecular dynamics simulations found increased packing fraction of atoms whose topological diagram at ultrahigh pressures is similar to pyrite-type crystalline phase, although the formation of tetraclusters is prohibited in crystalline phase. This critical difference would be caused by the potential structural tolerance in the glass for distortion of oxygen clusters. Furthermore, expanded electronic band gap demonstrates that chemical bonds survive at ultrahigh pressure. This opens up the synthesis of novel topologically disordered dense oxide glasses.**

## I. INTRODUCTION

Silica ($SiO_2$) has been known as one of the most fundamental and abundant oxides in the Earth, which can be usually yielded as quartz, silica sand, or silica stone in high purity condition. Due to this ubiquitous availability and abundant resource around the world, $SiO_2$ has been extensively utilized as an industrially useful material. $SiO_2$ glass, with high corrosion resistance, high thermo-stability, and high optical transparency, is a prototype network-forming glass which can be easily synthesized by various methods and it is therefore widely used and a technologically important material. Polyamorphism in $SiO_2$ glass under pressure is one of the most fascinating and puzzling topics in condensed matter physics and glass science. Several experimental and theoretical studies have been conducted to clarify the details of polyamorphism[1] in $SiO_2$ glass under high pressure. However, due to the technical hurdles, the experimental studies have been limited to very low pressure conditions, which prevents from a precise understanding of the pressure effect.

Previous experimental studies on $SiO_2$ glass have shown anomalous behavior under lower pressures up to ~10 GPa, exhibiting elastic softening[2] and permanent densification[3]. Those densification-related properties are closely related to a topological transformation of the tetrahedral network[4] and compaction of a significant amount of interstitial cavities in the $SiO_2$ glass[5], rather than a change in the coordination number of silicon. At higher-pressure, transitions

to much denser state are attributed to changes in short- and intermediate-range ordering associated with the change in oxygen coordination around silicon. Although the details on the coordination state and the pressure conditions under which the coordination changes occur are still a matter of debate[6], it appears that the sixfold-coordinated structure is predominant at 40-45 GPa[7,8] subsequent to a gradual change in the Si-O coordination number from four to six, which begins around 10-20 GPa[8], as inferred by a number of experimental measurements including Raman scattering[9], infrared absorption[10], X-ray diffraction/absorption[7,8,11,12], Brillouin scattering[13,14], X-ray Raman scattering[15], and neutron diffraction measurements[16]. Sato and Funamori[17] have reported that the coordination number of $SiO_2$ glass remains six at least up to 100 GPa based on the energy dispersive X-ray diffraction measurements, indicating that $SiO_2$ glass behaves as the corresponding crystalline phase with sixfold-coordinated structure between 40 and 100 GPa.

Ultrahigh-pressure acoustic wave velocity measurements on $SiO_2$ glass up to 207 GPa by Brillouin scattering spectroscopic experiment[18] have revealed an anomalous increase in the effect of pressure on acoustic velocity at ~140 GPa, which was interpreted as a structural transition from sixfold to higher coordination state of silicon above 140 GPa. A series of computational simulations on $SiO_2$ glass[19,20] have been conducted subsequently, and they have shown the possible formation of a Si-O coordination state higher than six under ultrahigh-pressure conditions above 100 GPa, which strongly support the experimental findings[18]. These results suggest that the $SiO_2$ glass becomes far denser under ultrahigh-pressure conditions than previously envisioned[7,8,17], which significantly reshapes our understanding on the nature of the densification mechanism of $SiO_2$ glass[1]. However, the change in acoustic wave velocity profile as a function of pressure only indicates a structural anomaly, while it does not provide us with any quantitative structural information. Therefore, it still remains experimentally unresolved whether or not such an anomalous increase in the acoustic velocity at ~140 GPa corresponds to a structural change associated with the coordination number increase. In addition, it has been believed that sixfold coordination state in crystalline $SiO_2$ retains at least above ~700 GPa. Clarifying this issue is thus also important for understanding the analogy between polymorphism and polyamorphism in silica systems under ultrahigh pressures. Very recently Prescher *et al.* performed high-pressure X-ray diffraction measurements up to 174 GPa and confirmed that average coordination number is greater than six at ultrahigh pressures[21], but atomic structure beyond the first coordination distance nor electronic structure is still unknown.

Here, we report the results of state-of-art topological analysis on the basis of atomic configuration obtained by classical molecular dynamics (MD) simulations and density functional theory (DFT) calculations up to 200 GPa. *In-situ* synchrotron high-pressure X-ray diffraction measurements support the reliability of simulation. Our supporting analytical methods include the concept of persistent homology[22], and we have placed a special focus on the nature of atomic structure, topology and electronic structures as a function of pressure. Furthermore, we have put emphasis on general understanding of pressure-induced modification in glass structure at atomistic and electronic level to illustrate a motif for densification in comparison with crystalline phases.

## II. EXPERIMENT

### A. X-ray diffraction measurements

We performed high-pressure *in-situ* X-ray diffraction measurements on the beamline BL10XU at the Japanese synchrotron facility of SPring-8[37]. Angle-dispersive high-pressure X-ray diffraction spectra were collected on the compressed $SiO_2$ glass at room temperature in a symmetric diamond anvil cell (DAC) at nine separate runs from 0 to 200 GPa. In each run, a pre-pressed plate of $SiO_2$ glass powder was loaded into a 50 to 100 μm hole, depending on the target pressure condition, drilled in the rhenium gasket without a pressure-transmitting medium. The sample was compressed with 300 μm flat culet and 150 μm beveled culet diamond anvils at lower five pressures and higher four pressures, respectively. The DAC with a large conical angular aperture used in the present experiments allowed the reliable diffraction patterns to be taken in a large angle up to a maximum 2 of 42˚. Pressure was determined using the Raman $T_{2g}$ mode of the diamond anvil[38] or ruby fluorescence pressure scale[39]. An incident X-ray beam was monochromatized, using a diamond double-crystal monochromator, to a beam energy of 49.6 and 49.9 keV. The X-ray beam was collimated to ~40 m in diameter, and X-ray diffraction spectra of the sample were obtained by an image plate (Rigaku-RAXIS IV), which has 3000×3000 (pixel) dimensions with a pixel size of 100 (m) × 100 (m)[37]. Integration of the full-circle scattered X-ray images was performed to give conventional one-dimensional scattered profiles. To subtract the background signals derived mainly from the Compton scattering of the diamond anvils, the background X-ray diffraction pattern was collected for each experimental run after decompression from an empty rhenium gasket hole in a diamond anvil cell after removal of the compressed sample. The $Q$ scale was calibrated using the diffraction pattern from the crystalline $CeO_2$. Density value of $SiO_2$ glass under high pressure, which is a key parameter in interpreting measured X-ray diffraction data, was estimated based on the recent results by an X-ray absorption

method[7]. The collected data were corrected and normalized to give Faber-Ziman structure factor using a standard program[40].

### B. MD simulation

Molecular dynamics (MD) calculations were performed with Born-Mayer type of pairwise potentials. The potentials of the term of Coulomb interactions with the effective charges of Si and O atoms and the repulsive term described by the exponential functions are calculated by the formula

$$\Phi_{ij} = \frac{e^2}{4\pi\varepsilon_0}\frac{Z_i Z_j}{r_{ij}} + B\exp\left(-\frac{r_{ij}}{\rho}\right)$$

where $r_{ij}$ is the interatomic distance between atoms, $Z$ is the effective charge, $B$ is the repulsive parameter, $e$ is elementary charge, $_0$ is permittivity of vacuum, and $\rho$ is the softness parameter. Supplementary Table 4 gives the parameters for $Z$, $B$ and $\rho$.

The present calculations were carried out for a system of 3,000 (1,000 Si + 2,000 O) atoms in the unit cell. The volume of the unit cell was determined from the number densities of the $SiO_2$ glasses under pressures of 10, 31, 46, 83, 109, 140, 170 and 200 GPa. Periodic boundary conditions were used and the long-range Coulomb interaction was treated with Ewald's summation. A time step of 1 fs was used in the Verlet algorithm. The program code for MD simulation was created by ourselves.

In the MD simulation, the structural models at different pressures were obtained from random starting atomic configurations. The temperature of the system was kept first at 4,000 K for 20,000 time steps, after which the system was cooled down to 293 K during 200,000 time steps. The structural model was finally annealed at 293 K for 20,000 time steps. Five structural models were prepared by repeating the above procedure for the different initial configurations for each condition.

We tested also other classical force fields with the LAMMPS program [http://lammps.sandia.gov]. The different parameterizations included the ReaxFF[41], COMB[42], CHIK[43] and BKS potentials[44] None of these worked properly in terms of density and atomic structure under high pressure of 109 GPa. This analysis highlights the intrinsic limitations present in the current interatomic potentials.

### C. Topological analysis

## 1. Cavity analysis

The cavity analysis has been performed as described in the previous literature[45]. The system is divided into a cubic mesh with a grid spacing of 0.10 Å, and the points farther from any atom at a given cutoff (here 2.1 Å, and 2.5 Å) are selected and defined as "cavity domains". Each domain is characterized by a center point where the distance to all neighboring atoms is maximal. The distance cutoff can be varied case-by-case, and the obtained results (volumes) depend closely on this value.

## 2. Persistent homology and persistent diagram

Given a set of points in the space, the persistent homology captures its topological multiscale structures, and those identified structures are compactly expressed in the format called persistent diagram. The construction of the persistent diagram follows the process described in Fig. 1a. We first replace each point with a sphere and increase its radius from zero to sufficiently large value. This process corresponds to changing resolution of our input data. Then, we record the pair of radii *(b,d)* at which a void (interstitial, vacancy, cavity) in a specific location appears (birth) and disappears (death), respectively. The persistent diagram is a histogram on the birth-death plane counting of voids at the coordinate *(b,d)*. From this construction, the persistent diagram enables not only to count the number of voids but also to characterize those shapes and multiscale properties. To provide readers' a better understanding of persistence diagrams, we show some examples of birth-death pairs for typical regular structures in Fig.1(b)-(e). For a regular hexagonal points whose distance between points is $a$, the void appears at radius $a/2$ and disappears at radius $a$ as shown in Fig. 1(b). For a regular triangular configuration, the void appear at $a/2$ and disappears at $\sqrt{1/3}a \approx 0.577a$ as shown in Fig. 1(c), and the 1-dimensional persistence diagram for a regular hexagonal/triangular points is shown in Fig. 1(d). For a 2-dimensional persistence diagram, we can similarly evaluate the cavities for a regular tetrahedron and octahedron. The birth and death radii are $\sqrt{1/3}a \approx 0.577a$ and $\sqrt{3/8}a \approx 0.612a$ for tetrahedron, and $\sqrt{1/3}a \approx 0.577a$ and $\sqrt{1/2}a \approx 0.707a$ for octahedron, and they are shown in Fig. 1(e). Therefore, the 2-dimensional persistence diagram of FCC crystal with a bond length $a$ displays two sharp peaks at $(0.577a, 0.612a)$ and $(0.577a, 0.707a)$ corresponding to two types of voids, interstitial tetrahedral and octahedral sites. For further details, we refer the reader to the article on persistent homology[22]. In our work, persistent diagrams are being used for investigating rings and polyhedral formations in atomic configurations. We also note that the detected rings and cavities are recorded during the

computation of persistent diagrams, and hence we can explicitly identify their geometric shapes for further analysis.

### D. DFT simulations

The CP2K program[46,47] was used to perform the DFT simulations of selected snapshot systems. CP2K employs two representations of the electron density: localized Gaussian and plane wave (GPW) basis sets. For the Gaussian-based (localized) expansion of the Kohn–Sham orbitals, we use a library of contracted molecularly optimized valence double-zeta plus polarization (m-DZVP) basis sets[48], and the complementary plane wave basis set has a cutoff of 550 Rydberg for electron density. The valence electron–ion interaction is based on the norm-conserving and separable Goedecker-Teter-Hutter (GTH) pseudopotentials[49]. The exchange–correlation energy functional is employs the generalized gradient corrected approximation of Perdew, Burke, and Ernzerhof (PBE)[50]. The DFT simulations were performed using a simulation box with 3,000 atoms where the starting geometry was constructed by the MD simulation mentioned above. The electronic density of states (DOS) and those with projections onto different elements (P-DOS) were calculated after atomic structure relaxation in a fixed volume (pressure). For each element, the effective volumes and charges were estimated from the atomic configuration and the electron density distribution based on the Voronoi method.

## III. RESULSTS and DISCUSSIONS

### A. Structural factors and real-space function

Fig. 2a shows the X-ray total structure factors $S(Q)$ measured up to 200 GPa, together with the $S(Q)$ derived from the MD simulations. The experimental $S(Q)$ are remarkably well reproduced by the MD simulation, although the height of the first sharp diffraction peak (FSDP) observed at 1.5 $Å^{-1} < Q < 2.7$ $Å^{-1}$ is slightly overestimated in the simulations (especially for 10 GPa). The observed FSDP position (see Table S1 in the Supplemental Materials [51]) shows a drastic and almost linear increase up to 31 GPa, and the FSDP profile becomes much more subtle beyond this point, which is in excellent agreement with the previous studies at least up to 100 GPa[7,8,12,17]. The second principal peak (PP) observed around $Q$ ~3 $Å^{-1}$, which has previously been considered as a manifestation of the presence of octahedrally (sixfold) coordinated Si[12], becomes prominent above 31 GPa, and the peak position gradually shifts to a higher $Q$ region with increasing pressure up to 170 GPa. As shown in Fig. 2b, this behavior is well understood in terms of partial structure

factors, $S_{\alpha\beta}(Q)$, in which the evolution of silicon-silicon principal peak increases with increasing pressure.

To understand the short-range structure in detail, the average Si-O bond length as a function of pressure was determined based on the first $T(r)$ peak position as well as the MD simulations in real space (Fig. S1 in the Supplemental Materials [51]), and the numerical values are shown in Fig. 3 together with the previous results[8,12,17]. Although there are some differences due to pressure conditions and insufficient real-space resolution in experimental data (especially above 83 GPa), the same trend of the Si-O bond lengths is observed among the experimental and MD simulations results. The results indicate that the average Si-O distance increases monotonically with pressure at least up to 46 GPa and turns to decline to 140 GPa, and eventually becomes constant up to 200 GPa. The overall trend of our results is consistent with those of Sato and Funamori[17] up to ~100 GPa and Prescher *et al.* up to 174 GPa[21]. According to the estimated bond lengths of six-fold coordinated crystalline $SiO_2$ phase[23] shown as the shaded area in Fig. 3, we suggest that the sixfold-coordinated silicon in $SiO_2$ glass becomes predominant at pressure approaching to 40 GPa.

Intermediate-range ordering in $AX_2$ glasses is of particular interest, because the typical examples of $SiO_2$ and $GeO_2$ are very well known as glass forming materials according to Zachariasen's theory[31]. Therefore, it is indispensable to investigate the relationship between the intermediate-range / chemical ordering and the behavior of the FSDP / the second PP in the structure factor. Although the MD simulations overestimate the FSDP heights, those observed for $S_{SiSi}(Q)$ and $S_{OO}(Q)$ appear to disappear at 31 GPa (Fig. 2b). Another remarkable feature is the very sharp PP observed at $Q \sim 2.75$ Å in $S_{SiSi}(Q)$, which is also observed in X-ray diffraction data (see Fig. 2a). The PP is usually observed at $Q \sim 3$ Å$^{-1}$ in neutron diffraction data at ambient to low pressures, because it reflects the packing of oxygen atoms[29,32]. However, our analyzed data suggest that the very intense PP in the X-ray diffraction data is a signature of increased packing fraction of silicon associated with the formation of tricluster and tetracluster configurations while the PP in $S_{OO}(Q)$ do not change significantly (Fig. 2b). These observations show a clear tendency for the pressure-induced deformation of intermediate-range topological ordering associated with chemical ordering manifested by the evolution of PP. Such a significant diminution of FSDPs with pressure is likely associated with the possible disturbance of the evolution of intermediate-range ordering caused by the pressure-induced diversification of coordination states and polyhedral linkages including an edge-shared connection observed in liquid $ZrO_2$[33].

**B. Si-O coordination numbers**

The distributions of Si-O coordination numbers were derived from the MD models and are shown in Fig. 2c where the gradual changes from fourfold to higher coordination can be clearly observed. The fourfold-coordinated structure retains up to 10 GPa almost as a single coordination species. The fivefold-coordinated structure becomes predominant at 31 GPa. The dominant coordination state subsequently shifts to sixfold at the pressure regime between 46 and 109 GPa. Here, a significant rise in the proportion of sevenfold coordination is visible, whereas the fraction of fivefold-coordinated configuration decreases as a compensation. Such a coordination number change with pressure is in a good agreement with the previous results up to 109 GPa[8,12,17] and up to 174 GPa[21]. However, it is found for the first time that the fraction of the sevenfold coordination state increases up to 40 % at 140 GPa, and becomes eventually greater than that of sixfold above 170 GPa reaching a fraction of 53 % at 200 GPa. The remarkable feature shown here is that the $SiO_2$ glass does not comprise a single coordination state under pressure but exhibits a broader distribution above 31 GPa, such as $SiO_6$ and $SiO_7$ polyhedra. Furthermore, the average coordination number is found to change gradually as the coordination distributions evolve. While the observed declining trend in the Si-O bond length at pressures approaching 140 GPa indicates a stable sixfold coordination state which behaves as the crystalline form of silica, the trend above 170 GPa showing the constant value can be interpreted as the onset of the average coordination number higher than 6. The corresponding snapshot of the local environment around oxygen atoms at 200 GPa constructed based on the MD simulation (Fig. 4a) highlights the formation of tricluster ($OSi_3$) and/or tetracluster ($OSi_4$) configurations that have never been reported previously. Furthermore, Voronoi polyhedral analysis[24] also implies the formation of the $SiO_6$ and $SiO_7$ polyhedra. With a careful inspection of such polyhedral atomic configurations, we find that the Si-O polyhedra exhibit a large variety of distorted features which deviate from the ideal regular polyhedral structures, as shown in Fig. S2 in the Supplemental Materials [51].

### C. Bond angle distribution and polyhedral connection

To uncover the atomic structure in $SiO_2$ glass at high pressures, we have calculated bond angle distributions with pressure, and they are shown as O-Si-O and Si-O-Si configurations in Fig. 4b. The O-Si-O bond angle distribution at 0 GPa shows a fairly sharp maximum close to 109.4˚ as expected for a regular $SiO_4$ tetrahedron. The maximum peak position gradually gets smaller down to ~90˚ up to 83 GPa, and the peak distribution becomes distorted with a broad shoulder at larger angles above ~110˚. Although the sixfold-coordinated structure is presumed to be the major component at 83 GPa, the corresponding angle distributions largely deviate from the ideal O-Si-O

angle of 90˚ for a regular octahedron. The broad feature is consistent with the broad Si-O coordination number distribution at high pressure (Fig. 2c), suggesting that the changes in bond angle distributions are due to the wide variety of O coordination around Si at high pressures.

The features of O-Si-O bond angles at 200 GPa distinctively differ from those observed at lower pressures. The peaks around 75˚ and 145˚ are highly analogous to those observed in the random packing structure of hard spheres, indicating that the structure of $SiO_2$ glass under ultrahigh pressure is very different from that at ambient pressure. Taken into account our results for the short-range structure, the appearance of such peak/shoulders correlates with the formation of sevenfold or higher coordinated structures in a highly-distorted polyhedral geometry which is in line with the results of Voronoi analysis.

The Si-O-Si bond angle distribution shows a peak towards 180˚ up to 10 GPa, which is a signature of tetrahedral network. On the other hand, the position of the peak shift to small angle region from 31 GPa and shows two peaks around 103˚ ($OSi_4$ tetracluster) and 124˚ ($OSi_3$ tricluster) at 140 GPa. The latter peak is not obvious at 200 GPa, suggesting that $OSi_4$ tetracluster becomes more dominant.

In order to shed further light on the nature of the atomic arrangement, the total volume of cavities ("voids") and polyhedral connections for $SiO_n$ polyhedra were calculated, and are summarized in Table S2 in the Supplemental Materials [51]. The fraction of cavity volumes exhibits drastic decrease with pressure and there are essentially no cavities above 31 GPa, while the $SiO_2$ glass initially has a cavity volume of 36.8% at ambient pressure. Previously, it has been considered that the presence of interstitial cavities in the $SiO_2$ glasses/melts indicates a potential ability to store noble gases, such as helium and argon, within the disordered structures[25]. The rapid decrease in the cavity volume with pressure approaching 30 GPa offers a feasible explanation for the observation in the previous high-pressure experiments where the solubility of noble gases in $SiO_2$ melts/glasses drastically decreased at pressures around 10-20 GPa[25].

Table S2 and Figure S3 in the Supplemental Materials [51] also show the pressure-induced change in the polyhedral connections for $SiO_n$. The connections initially display 100% of corner-shared configurations at ambient pressure, and they show a gradual transition from corner-shared to edge-shared structures together with a minor fraction of face-shared structures.

### D. Topological nature

To elucidate the structural information that cannot be sufficiently analyzed by the conventional methods from atomic configurations, we applied a topological/mathematical method using

persistent homology for characterizing the geometrical features in amorphous materials[22]. This method is primarily based on the persistent diagram (PD) which can visualize the persistent homology 2-dimensionally, and thus various topological features such as ring structures and polyhedral connections/distortions can be monitored.

Figs. 5a-g show Si-centric PDs $D(\mathrm{Si})_1$ which describe the geometrical features of silicon atoms for the topological dimensionality of 1. We compare 0, 31, 83, and 200 GPa data together with stishovite ($d$=4.28 g/cm$^3$)[26], α-$PbO_2$ type ($d$=4.30 g/cm$^3$) [27], and pyrite type ($d$=6.58 g/cm$^3$) [28]. With those PDs, we can extract the geometrical information of the atoms primarily associated with the 1-dimensional linkages such as rings. The profiles along with the death line highlighted by colors are shown in Fig. 5h. In the case of crystalline phase, we can observe systematic peak shift to small death value with increasing density. It is found that a vertical and broad profile along with the death line observed at birth = 2.6 Å$^2$ at ambient pressure in glass almost disappears at 31 GPa and an intense profile in both vertical and horizontal appears near the diagonal line at birth ~ 3 Å$^2$. This behavior is a good descriptor for FSDP and is consistent with the observation of tricluster and tetracluster configurations under high pressures. Furthermore, peak of glass at 200 GPa is very close to pyrite-type data, although density of the glass is much smaller than the crystalline phase. Similar behaviour is observed in O-centric PDs $D(\mathrm{O})_1$ shown in Fig. S4 in the Supplemental Materials [51].

Figs. S5a-g in the Supplemental Materials [51] shows Si-centric PDs $D(\mathrm{Si})_2$ of glasses and three crystalline phases, which describe the geometrical features of the silicon atoms for the topological dimensionality of 2. With those PDs, we can extract the geometrical information of the atoms primarily associated with the 2-dimensional connections such as polyhedral formation with the reduction of cavity volume. The geometrical configurations having all those characteristics observed above 31 GPa no longer represent a network structure but rather dense packed structure[22]. The profiles along with the diagonal line highlighted by colors are shown in Fig. S5h in the Supplemental Materials [51]. The birth value of broad prole along with the diagonal line rapidly decreases and multiplicity is increased with increasing pressure, which is in line with the behavior of $D(\mathrm{Si})_1$ (Fig. 5). In addition, the profile of glass at 200GPa is similar to that of pyrite-type crystalline phase. On the other hand, O-centric PDs $D(\mathrm{O})_2$ (Figs. 6a-g) show that some data initially distributed along the diagonal line at lower pressure get gradually deviated in a direction toward upper left from the diagonal line with pressure and, eventually, appear to form the isolated cluster-like "island" at 200 GPa apart from the original distribution. The profiles along with the death line highlighted by colors are shown in Fig. 6h, which shows similar

behavior with silicon atoms. With the analyses of persistent homology, the emergence of such "island-like" deviation is found to correspond to the formation of the octahedrally-coordinated oxygen atoms (that is $SiO_6$) whereas the distribution along the diagonal indicates the presence of the oxygen tetrahedra ($SiO_4$). This interpretation is remarkably compatible with our earlier findings. In addition, recent topological analyses for the metallic glass with highly dense-packed structure[21] also showed the very similar topological nature in PDs to that obtained under higher-pressure condition in this study, again indicating that the densification is achieved by the gradual transition from network structure to dense packed structure in conjunction with a change in the coordination state.

As can be seen in Fig. 2b, $S_{SiSi}(Q)$ is very sensitive to pressures above 31GPa, while that of the PP in $S_{OO}(Q)$ is highly insensitive, which is highly correlated with the pressure-induced changes in PDs $D_1$ and $D_2$, respectively. These behaviors are also very far away from those in densification at lower pressure reported by Zeidler et al[29]. Pressure-induced structural change in our study could therefore be categorized into the pressure-induced "topological disorder" in the intermediate length scale, associated with chemical ordering under ultrahigh pressure[34]. This implies that only high pressure can produce such an unusual glass structure at room temperature. Furthermore, our finding paves the way for the synthesis of novel families of highly-disordered, dense glasses from various oxides (including cases with low glass-forming ability) by applying ultrahigh pressure.

Recently, Zeidler et al[29] proposed a groundbreaking concept on the relationship between coordination numbers and oxygen packing fractions (OPF) in oxide glasses, which gives a universal picture of the coordination number evolution under pressure. This concept is highly supported by the recent high-pressure experimental results on $GeO_2$ glass up to 100 GPa[30], strengthening the predictability of this concept towards configurations under extreme pressures. According to the extrapolated calculations with some assumptions for OPF in $SiO_2$ glass from previous calculations[8,16,17], the onset pressure where the Si-O coordination number becomes higher than 6 is expected around 108 GPa[30]. This is consistent with the present results for OPFs up to 200 GPa shown in Fig. S6, and supports our previous results for sound velocity as well[18].

### E. DFT simulations

We have shown above that the $SiO_2$ glass undergoes a transition from network- to dense packed-structure in conjunction with the coordination number change under high-pressure. It is expected that most substances with a dense packed ultimately become metallic under extreme pressures, and the question arises whether the $SiO_2$ glass expresses metallic features under

ultrahigh-pressure conditions approaching 200 GPa. To address this issue and to reveal the effects of the changes in Si-O coordination number on electronic states, we computed the electronic structures of the $SiO_2$ glass by DFT calculations based on the structural models discussed above (samples of 3,000 atoms, fixed volume). The DFT results for the effective charges ($Q_{eff}$) and atomic volumes ($V_{at}$) of Si and O atoms are listed in Table S3 in the Supplemental Materials [51]. The effective charges are remarkably insensitive to pressure exhibiting values close to +2 for Si and -1 for O. On the other hand, the atomic volume of Si appears to decrease monotonically with pressure, whereas the same for O shows a drastic reduction of as much as 50 % within the pressure range 0 - 31 GPa. Since the atomic volume is mainly assigned to O within the Voronoi script, this significant reduction of atomic volumes of O with no changes in the electronic structure and effective charges corresponds to the disappearance of cavity volumes between 0-31 GPa (Table S2 in the Supplemental Materials [51]) as described above. The reduced volume of O together with the disappearing cavities stimulates the formation of $SiO_6$ from $SiO_4$, which is also observed to have its onset around 30 GPa. Owing to such rapid changes in $V_{at}$, the O and Si volumes approach each other at higher pressures supporting, again, the conclusion that $SiO_2$ glass undergoes structural changes in line with the hard-sphere-like dense packing without any metallic signature.

The electronic structure of $SiO_2$ glass under pressure was analyzed based on the electronic density of states (DOS). Fig. 7 shows the DOS of $SiO_2$ glass with projections onto different elements, P-DOS. The distribution of the P-DOS bands is found to become broader with increasing pressure, which reflects the wider distribution of the oxygen coordination number around silicon under high pressures. Despite these changes, the band gaps at the Fermi energy become wider with pressure as shown in Fig. 7, implying that the system remains insulating under pressure. The structural diversity has normally been considered to make the band gap narrower[33], which seems contradictory to the fact that our results shows apparent structural varieties with pressure. One possible reason may be the increase in bond angle symmetry for Si-O-Si whereas the symmetry of O-Si-O decreases with pressure, as can be seen in Fig. 4b. If this is the case, the formation of over-coordinated oxygen with relatively symmetric bond angles may secure the insulation property of the $SiO_2$ glass under high pressure.

To manifest the topology in silica glass under ultrahigh-pressures, we extract the atomic configurations which give an intense multiplicity for $D(\mathrm{Si})_1$ and $D(\mathrm{Si})_2$ of pyrite-type crystal and glass at 200 GPa and show in Fig. 8(a) and (b), respectively. Intriguingly, PD analyses can provides us with information about triclusters and tetraclusters from $D(\mathrm{Si})_1$ and $D(\mathrm{Si})_2$,

441 respectively. Pyrite-type crystal is comprised of only $SiO_6$ octahedra ($OSi_3$ tricluster). On the
442 other hand, the formation of a $SiO_7$ polyhedron is observed in glass as well as $SiO_6$ octahedra, but
443 its topology is very similar to pyrite-type crystal (see Fig. 8a). As can be seen in Fig. 8(b),
444 tricluster in pyrite-type crystal can be extracted from PD analysis (see left panel), while the
445 formation of $OSi_4$ tetracluster is observed in glass at 200 GPa (right panel). However, it is found
446 that tetracluster is highly distorted (oxygen atom is off center) and topology is very similar to $OSi_3$
447 + Si, in pyrite-type crystal. We suggest that the topological similarity between glass at 200 GPa
448 and pyrite-type crystal would be caused by the distortion of oxygen clusters and the variety of
449 Si-O coordination in terms of disorder in glass.
450

451 **IV. CONCLUSIONS**

452 In this article, we have investigated the topology of $SiO_2$ glass MD simulations supported by
453 using the high-energy synchrotron X-ray diffraction technique and topological analyses in a
454 pressure range up to 200 GPa. Our results reveal that the $SiO_2$ glass undergoes a coordination
455 number change from six to seven at pressure approaching 200 GPa. The atomistic modelling
456 demonstrates the formation of unusual densely arranged local structures around O atoms, such as
457 tricluster ($OSi_3$) or tetracluster ($OSi_4$) configurations. The topological analyses succeed in
458 visually discriminating the Si-O coordination changes between fourfold and sixfold using PDs,
459 and reveal that the high-pressure form of the $SiO_2$ glass exhibits highly distorted structural
460 features, which have so far been unable to be seen by the use of incoherent X-rays and of the
461 conventional analysis tools with defining coordination distances (pair correlation function, bond
462 angle distribution, and so on). Furthermore, we observed the topological similarity between glass
463 and crystal with higher density under ultrahigh-pressure for the first time. This also strongly
464 offers a new direction in the future experiment to determine hidden local symmetries in pair
465 correlation by cross-correlation analysis employing coherent X-rays[35]. The results also
466 demonstrate that the coordination number change of $SiO_2$ glass no longer follows that of the
467 crystalline $SiO_2$ phase under ultrahigh pressures since the sixfold-coordinated structure is
468 believed to persist, at least, up to ~700 GPa for the latter case[36]. The evolution of Si-O
469 coordination number appears to remarkably follow the universal path for OPF with pressure, as
470 proposed by Zeidler et al[29]. This pronounced difference between the glass and crystalline phase in
471 pressure-induced structural change is most likely caused by the potential structural tolerance in
472 the glass for accepting the distortion to certain extent, which might allow the glasses to have

unusually higher coordination numbers that cannot be achieved in crystalline phase at equivalent condition.

**References and Notes**


1 El'kin, F. S., Brazhkin, V. V., Khvostantsev, L. G., Tsiok, O. & Lyapin, A. G. In situ study of the mechanism of formation of pressure-densified $SiO_2$ glasses. *J. Exp. Theor. Phys. Lett.* **75**, 342-347 (2002).

2 Bridgman, P. W. The compressibility of several artificial and natural glasses. *Am. J. Sci.* **10**, 359-367 (1925).

3 Bridgman, P. W. The Effect of Pressure on the Tensile Properties of Several Metals and Other Materials. *J. Appl. Phys.* **24**, 560-570, doi:Doi 10.1063/1.1721329 (1953).

4 Trachenko, K. & Dove, M. T. Compressibility, kinetics, and phase transition in pressurized amorphous silica. *Phys. Rev. B* **67**, Doi 10.1103/Physrevb.67.064107 (2003).

5 Shackelford, J. F. & Masaryk, J. S. The interstitial structure of vitreous silica. *J. Non. Cryst. Solids* **30**, 127-134 (1978).

6 Lacks, D. J. First-order amorphous-amorphous transformation in silica. *Phys. Rev. Lett.* **84**, 4629-4632, doi:DOI 10.1103/PhysRevLett.84.4629 (2000).

7 Sato, T. & Funamori, N. Sixfold-Coordinated Amorphous Polymorph of $SiO_2$ under High Pressure. *Phys. Rev. Lett.* **101**, Firist-last page, Doi 10.1103/Physrevlett.101.255502 (2008).

8 Benmore, C. J., Soignard,E., Amin, Guthrie, S. A., Shastri, M. S., Lee, D. P. L. & Yarger, J. L. Structural and topological changes in silica glass at pressure. *Phys. Rev. B* **81**, Firist-last page, Doi 10.1103/Physrevb.81.054105 (2010).

9 Hemley, R. J., Mao, H. K., Bell, P. M. & Mysen, B. O. Raman-Spectroscopy of $SiO_2$ Glass at High-Pressure. *Phys. Rev. Lett.* **57**, 747-750, doi:DOI 10.1103/PhysRevLett.57.747 (1986).

10 Williams, Q. & Jeanloz, R. Spectroscopic Evidence for Pressure-Induced Coordination Changes in Silicate-Glasses and Melts. *Science* **239**, 902-905, doi:DOI 10.1126/science.239.4842.902 (1988).

11 Inamura, Y., Katayama, Y., Utsumi, W. & Funakoshi, K. Transformations in the

intermediate-range structure of $SiO_2$ glass under high pressure and temperature. *Phys. Rev. Lett.* **93**, Firist-last page, Doi 10.1103/Physrevlett.93.015501 (2004).

12 Meade, C., Hemley, R. J. & Mao, H. High-pressure X-ray diffraction of $SiO_2$ glass. *Phys. Rev. Lett.* **69**, 1387 (1992).

13 Grimsditch, M. Polymorphism in Amorphous $SiO_2$. *Phys. Rev. Lett.* **52**, 2379 (1984).

14 Zha, C.-s., Hemley, R. J., Mao, H.-k., Duffy, T. S. & Meade, C. Acoustic velocities and refractive index of $SiO_2$ glass to 57.5 GPa by Brillouin scattering. *Phys. Rev. B* **50**, 13105 (1994).

15 Lin, J.-F., Fukui, H., Prendergast, D., Okuchi, T., Cai, Y. Q., Hiraoka, N., Yoo, C-S., Trave, A., Eng, P., Hu, M. Y. & Chow, P. Electronic bonding transition in compressed $SiO_2$ glass. *Phys. Rev. B* **75**, 012201 (2007).

16 Zeidler, A., Wezka, K., Rowlands, R. F., Whittaker, D. A. J., Salmon, P. S., Polidori, A., Drewitt, J. W. E., Klotz, S., Fischer, H. E., Craig, M. C. W., Tucher, M-G. and Wilson, M. High-pressure transformation of $SiO_2$ glass from a tetrahedral to an octahedral network: a joint approach using neutron diffraction and molecular dynamics. *Phys. Rev. Lett.* **113**, 135501 (2014).

17 Sato, T. & Funamori, N. High-pressure structural transformation of $SiO_2$ glass up to 100 GPa. *Phys. Rev. B* **82**, 184102 (2010).

18 Murakami, M. & Bass, J. D. Spectroscopic evidence for ultrahigh-pressure polymorphism in $SiO_2$ glass. *Phys. Rev. Lett.* **104**, 025504 (2010).

19 Brazhkin, V., Lyapin, A. & Trachenko, K. Atomistic modeling of multiple amorphous-amorphous transitions in $SiO_2$ and $GeO_2$ glasses at megabar pressures. *Phys. Rev. B* **83**, 132103 (2011).

20 Wu, M., Liang, Y., Jiang, J.-Z. & John, S. T. Structure and properties of dense silica glass. *Sci. Rep.* **2**, 398 (2012).

21 Prescher, C., Prakapenka, V. B., Stefanski, J., Jahn, S., Skinner, L. B. & Wang Y. Beyond sixfold coordinated Si in $SiO_2$ glass at ultrahigh pressures. *Proc. Natl. Acad. Sci. U.S.A.* **114** (38) 10041-10046 (2017)

22 Hiraoka, Y., Nakamura, T., Hirata, A., Escolar, E. G., Matue, K. & Nishiura, Y. Hierarchical structures of amorphous solids characterized by persistent homology. *Proc. Natl. Acad. Sci. U.S.A.* **113**, 7035-7040 (2016).

23 Andrault, D., Fiquet, G., Guyot, F. & Hanfland, M. Pressure-induced Landau-type transition in stishovite. *Science* **282**, 720-724 (1998).

24 Fukunaga, T., Itoh, K., Otomo, T., Mori, K., Sugiyama, M., Kato, H., Hasegawa, M., Hirata, A., Hirotsu, Y. & Hannon, A. C. Voronoi analysis of the structure of Cu–Zr and Ni–Zr metallic glasses. *Intermetallics* **14**, 893-897 (2006).

25 Paonita, A. Noble gas solubility in silicate melts: a review of experimentation and theory, and implications regarding magma degassing processes. *Ann. Geophys.* (2005).

26 Ross, N. L., Shu, J. & Hazen, R. M. High-pressure crystal chemistry of stishovite. A*m. Mineral.* **75** (7-8): 739–747 (1990)

27 Dera, P., Prewitt, C. T., Boctor, N. Z. & Hemley, R. J. Characterization of a high-pressure phase of silica from the Martian meteorite Shergotty. A*m. Mineral.* **87** (7): 1018–1023 (2002)

28 Kuwayama, Y., Hirose, K., Sata, N. & Ohishi, Y. The pyrite-type high-pressure form of silica. *Science* **309**, 923-925 (2005)

29 Zeidler, A., Salmon, P. S. & Skinner, L. B. Packing and the structural transformations in liquid and amorphous oxides from ambient to extreme conditions. *Proc. Natl. Acad. Sci. U.S.A.* **111**, 10045-10048 (2014).

30 Kono, Y., Kenney-Benson, C., Ikuta, D., Shibazaki, Y., Wang, Y. & Shen, G. Ultrahigh-pressure polyamorphism in $GeO_2$ glass with coordination number> 6. *Proc. Natl. Acad. Sci. U.S.A.* 201524304 (2016).

31 Zachariasen, W. H. The atomic arrangement in glass. *J. Am. Chem. Soc.* **54**, 3841-3851 (1932).

32 Zeidler, A. & Salmon, P. S. Pressure-driven transformation uof the ordering in amorphous network-forming materials. *Phys. Rev. B* **93**, 214204 (2016).

33 Kohara, S., Akola, J., Patrikeev, L., Ropo, M., Ohara, K., Itou, M., Fujiwara, A., Yahiro, J., Okada, J. T., Ishikawa, T., Mizuno, A., Masuno, A., Watanabe, Y. & Usuki, T. Atomic and electronic structures of an extremely fragile liquid. *Nat. Commun.* **5**, 5892 (2014).

34 Salmon, P. S., Barnes, A. C., Martin, R. A. & Cuello, G. J. Glass fragility and atomic ordering on the intermediate and extended range. *Phys. Rev. Lett.* **96**, 235502 (2006).

35 Wochner, P., Gutt, C., Autenrieth, T., Demmer, T., Bugaev, V., Ortiz, A. D., Duri, A., Zontone, F., Grubel, G. & Dosch, H. X-ray cross correlation analysis uncovers hidden local symmetries in disordered matter. *Proc. Natl. Acad. Sci. U.S.A.* **106**, 11511-11514 (2009).

36 Wu, S., Umemoto, K., Ji, M., Wang, C-Z., Ho, K-M. & Wentzcovitch, R. M. Identification of post-pyrite phase transitions in $SiO_2$ by a genetic algorithm. *Phys. Rev. B* **83**, 184102 (2011).

37 Ohishi, Y., Hirao, N., Sata, N., Hirose, K. & Takata, M. Highly intense monochromatic X-ray diffraction facility for high-pressure research at SPring-8. *High Press. Res.* **28**, 163-173 (2008).

38 Akahama, Y. & Kawamura, H. High-pressure Raman spectroscopy of diamond anvils to 250 GPa: Method for pressure determination in the multimegabar pressure range. *J. Appl. Phys.* **96**, 3748-3751 (2004).

39 Mao, H., Xu, J.-A. & Bell, P. Calibration of the ruby pressure gauge to 800 kbar under quasi‐hydrostatic conditions. *J.Geophys. Res.* **91**, 4673-4676 (1986).

40 Kohara S. et al., *Z. Phys. Chem.* **230(3)**, 339-368 (2016).

41 Van Duin, A. C., Dasgupta, S., Lorant, F., & Goddard, W. A.. ReaxFF: a reactive force field for hydrocarbons. *J. Phys. Chem.* **105**(41), 9396-9409 (2001).

42 Tzu-Ray Shan, Devine Bryce, Jeffery Hawkins, Aravind Asthagiri, Simon Phillpot, and Susan Sinnott. Second-generation charge-optimized many-body potential for Si/ $SiO_2$ and amorphous silica. *Phys. Rev. B*, **82**, 235302 (2010).

43 Horbach J., Molecular dynamics computer simulation of amorphous silica under high pressure. *J. Phys. Condens. Matter* **20**, 244118 (2008).

44 van Beest B. W. H., Kramer G. J., and van Santen R. A.. Force fields for Silicas and Aluminophosphates Based on Ab Initio Calculations. *Phys. Rev. Lett.* **64**, 1955–1958 (1990).

45 Akola, J. & Jones, R. Structural phase transitions on the nanoscale: The crucial pattern in the phase-change materials $Ge_2Sb_2Te_5$ and GeTe. *Phys. Rev. B* **76**, 235201 (2007).

46 VandeVondele, J., Krack, M., Mohamed, F., Parrinello, M., Chassaing, T. & Hutter, J. Quickstep: Fast and accurate density functional calculations using a mixed Gaussian and plane waves approach. *Comput. Phys. Commun.* **167**, 103-128 (2005).

47 Hutter, J., Iannuzzi, M., Schiffmann, F. & VandeVondele, J. CP2K: atomistic simulations of condensed matter systems. *Wiley Interdisciplinary Reviews: Computational Molecular Science* **4**, 15-25 (2014).

48 VandeVondele, J. & Hutter, J. Gaussian basis sets for accurate calculations on molecular systems in gas and condensed phases. *J. Chem. Phys.* **127**, 114105 (2007).

49 Goedecker, S., Teter, M. & Hutter, J. Separable dual-space Gaussian pseudopotentials. *Phys. Rev. B* **54**, 1703 (1996).

50 Perdew, J. P., Burke, K. & Ernzerhof, M. Generalized gradient approximation made simple. *Phys. Rev. Lett.* **77**, 3865 (1996).

51 See Supplemental Materials at [*URL*] for more information regarding the atomic, electronic, and topological nature of the $SiO_2$ glass under high pressure condition. The Supplemental Materials contain Refs. [8, 16, 17, 52-56]

52 Wezka, K., Salmon, P. S., Zeidler, A., Whittaker, D. A., Drewitt, W. E., Klotz, S., Fischer, H. E. & Marrocchelli, D. Mechanisms of network collapse in $GeO_2$ glass: high-pressure neutron diffraction with isotope substitution as arbitrator of competing models. *J. Phys. Condens. Matter* **24**, 502101 (2012).

53 Drewitt, J. W., Salmon, P. S., Barnes, A. C., Klotz, S., Fischer, H. E. & Crichton, W. A. Structure of $GeO_2$ glass at pressures up to 8.6 GPa. *Phys. Rev. B* **81**, 014202 (2010).

54 Salmon, P. S., Drewitt, J. W. E., Whittaker, D. A. J., Zeidler, A., Wezka, K., Bull, C. L., Tucher, M-G., Cilding, M. C., Guthrie, M. & Marrocchelli, D. Density-driven structural transformations in network forming glasses: a high-pressure neutron diffraction study of $GeO_2$ glass up to 17.5 GPa. *J. Phys. Condens. Matter* **24**, 415102 (2012).

55 Guthrie, M., Tulk, C. A., Benmore, C. J., Xu, J., Yarger, J. L., Klug, D. D., Tse, J. S., Mao, H-k & Hemley, R. J. Formation and structure of a dense octahedral glass. *Phys. Rev. Lett.* **93**, 115502 (2004).

56 Mei, Q., Sinogeikin, S., Shen, G., Amin, S., Benmore, C. J. & Ding, K. High-pressure x-ray diffraction measurements on vitreous $GeO_2$ under hydrostatic conditions. *Phys. Rev. B* **81**, 174113 (2010)

## Acknowledgments

**Funding:** The synchrotron radiation experiments were performed under the approval of the Japan Synchrotron Radiation Research Institute (JASRI) (Proposal No. 2009A1064, 2010A1048, 2010B1092, 2011A1239, 2011B1159, 2011B1153, 2013B1217). This research was supported by a Grant-in-Aid for Young Scientists (A) (#22684028), Challenging Exploratory Research (#24654170) and Scientific Research (A) (#25247087) from the Ministry of Education, Culture, Sports, Science and Technology, Japan, a Grant for Program Research from Frontier Research Institute for Interdisciplinary Sciences, Tohoku University, and the Start-up funds at ETH Zürich (to M.M.), This work was supported by JST PRESTO Grant Number JPMPR15N4, Japan (to S.K.) and “Materials research by Information Integration” Initiative (MI2I) project of the Support Program for Starting Up Innovation Hub from JST (to S.K. and

Y.H.). JST CREST 15656429 (to Y.H.). The DFT calculations were carried out on the Cray XT4/XT5 computers at CSC - the IT Center for Science Ltd., Finland, and Cray XC30 in Japan Advanced Institute of Science and Technology, Japan. J.A., J.K., T.M. and A.S.F. acknowledge financial support from the Academy of Finland through its Centres of Excellence Program (Project 284621).

**Author contributions:** M.M. and S.K. designed the research conception. M.M. and N.H. conducted *in-situ* high-pressure synchrotron X-ray diffraction experiments. S.K. performed the atomic structural analyses. H.I. constructed structural model using MD simulations. N.K. and J.A. contributed to the electronic structural analyses. A.H., Y.H. and I.O. were involved in the topological analyses. T.M., A.S.F and J.A tested various parameterizations of the interatomic potentials for MD simulation. N.H. and Y.O. contributed to the optimization of *in-situ* synchrotron X-ray diffraction measurements. Y. Onodera. calculated the OPFs. J.K. and J.A. contributed to the cavity analyses. O.S and Y.I. were involved in the data analyses for atomic and electronic structures, respectively.

**Competing interests:** Authors declare no conflict of interest.

## Figures and Tables

**Fig. 1**. (**a**) The increasing sequence of spheres for input data (left). The persistent diagram (right) is obtained as a histogram counting the number of voids on the birth-death plane. (**b-c**) The appearance and disappearance of a void for a regular hexagon/triangle. (**d**) The pairs of birth and death radii for hexagon and triangle in the 1-dimensional persistence diagram. (**e**) The pairs of birth and death radii for tetrahedron and octahedron in the 2-dimensional persistence diagram.

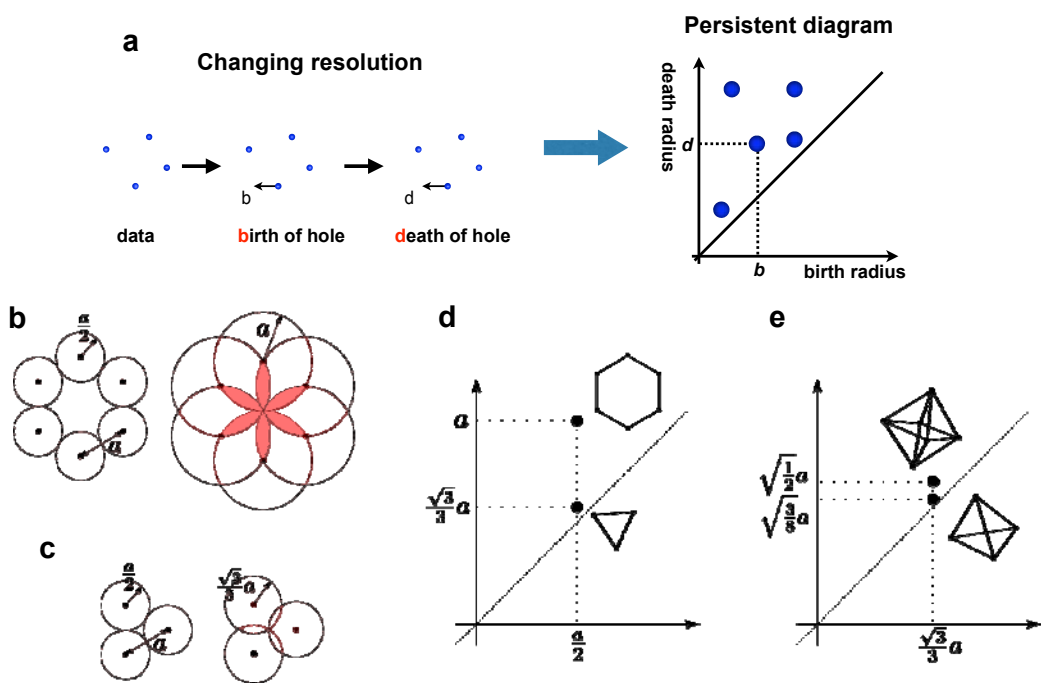

**Fig. 2 High-pressure structural data and pressure evolution of Si-O coordination number of $SiO_2$ glass.** (**a**) X-ray total structure factors $S(Q)$ of $SiO_2$ glass up to pressures of 200 GPa. Dotted curves, experimental data; solid curves, MD simulations. (b) Faber-Ziman partial structure factors of $S_{SiSi}(Q)$, $S_{SiO}(Q)$ and $S_{OO}(Q)$ up to 200 GPa. The approximate principal peak positions as labeled by $Q_1$, $Q_2$, and $Q_3$ observed under ambient condition are indicated by the vertical broken lines. (c) Distribution of the Si-O coordination number in $SiO_2$ glass as a function of pressure up to 200 GPa. Number in the square denotes the average Si-O coordination number at each pressure.

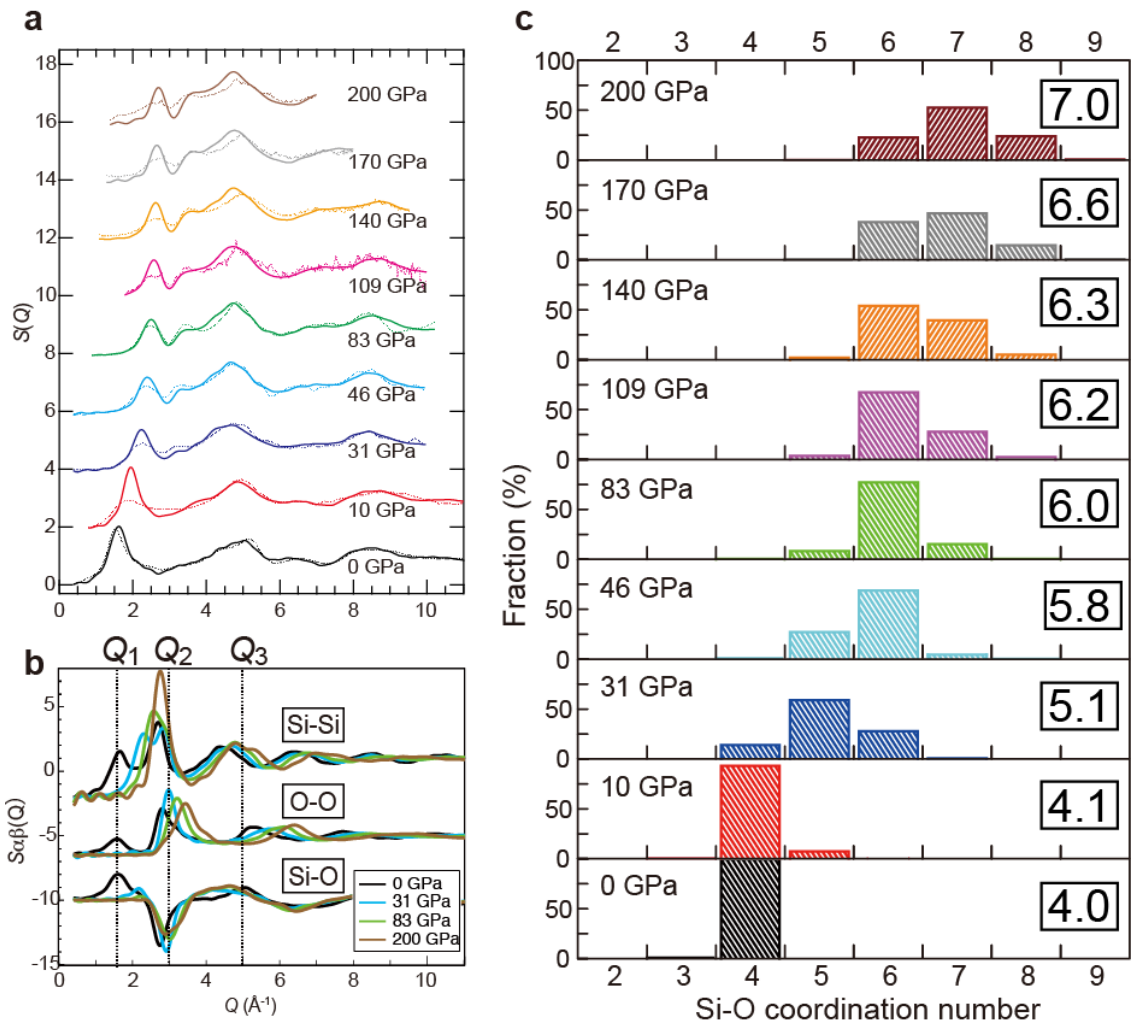

**Fig. 3** Pressure dependence of the Si-O bond length of silica glass up to pressures of 140 GPa together with the previous results[8,12,17, 21]. The shaded areas represent the range of Si-O bond lengths for crystalline silica phases with fourfold- and sixfold-coordinated[23] structures.

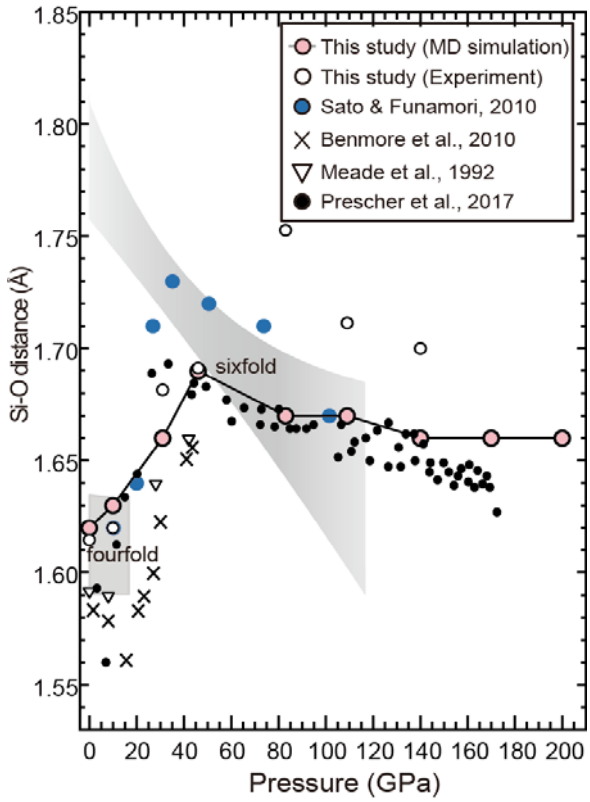

**Fig. 4. Atomic structure and bond angle distribution of $SiO_2$ glass under high-pressure.** (**a**) Snapshot of the local environment around oxygen atoms at 200 GPa, highlighting the oxygen tricluster and tetracluster configurations (O coordinated with three or four silicon). Blue spheres, silicon atoms; yellow spheres, oxygen atoms. (**b**) Pressure dependence of the O-Si-O (left), and Si-O-Si (right) bond angle distribution up to 200 GPa.

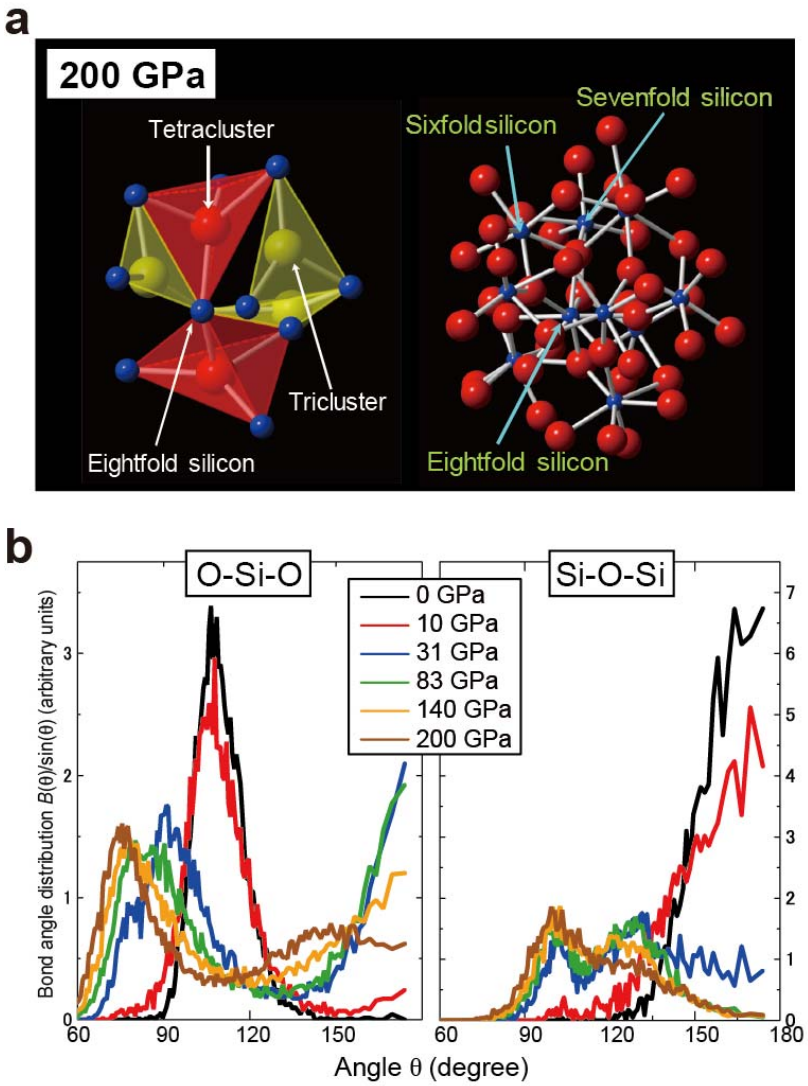

**Fig. 5. Analysis using Si-centric persistent homology for the topological dimensionality of 1.** (**a-g**) Si-centric Persistent diagrams $D(\mathrm{Si})_1$ at 0, 31, 83 and 200 GPa (**h**) The probability profiles along with the death line highlighted by colors. Black line, 0 GPa; blue line, 31 GPa, green line, 83 GPa, and brown line, 200 GPa. Light green, stishovite; pink, α-$PbO_2$-type $SiO_2$; gray, pyrite-type $SiO_2$.

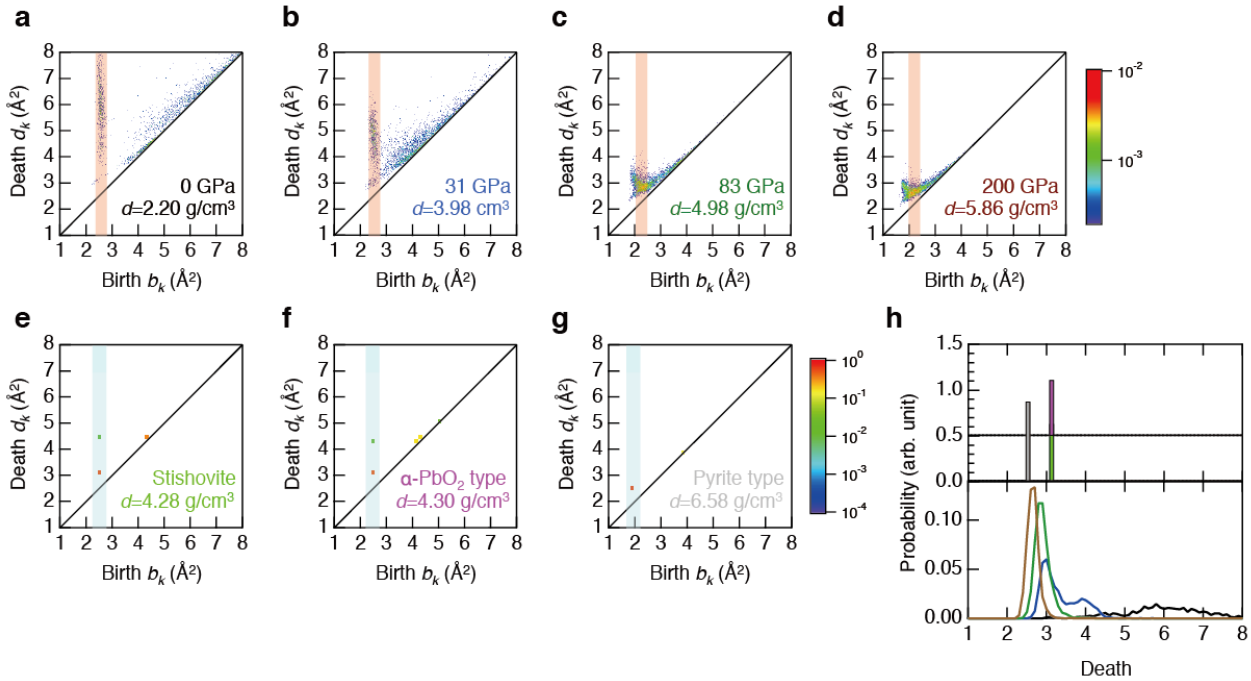

**Fig. 6. Analysis using O-centric persistent homology for the topological dimensionality of 2.** (**a-g**) O-centric persistent diagrams for $D(O)_2$ at 0, 31, 83 and 200 GPa (**h**) The probability profiles along with the diagonal line highlighted by colors. Black line, 0 GPa; blue line, 31 GPa, green line, 83 GPa, and brown line, 200 GPa. Light green, stishovite; pink, α-$PbO_2$-type $SiO_2$; gray, pyrite-type $SiO_2$.

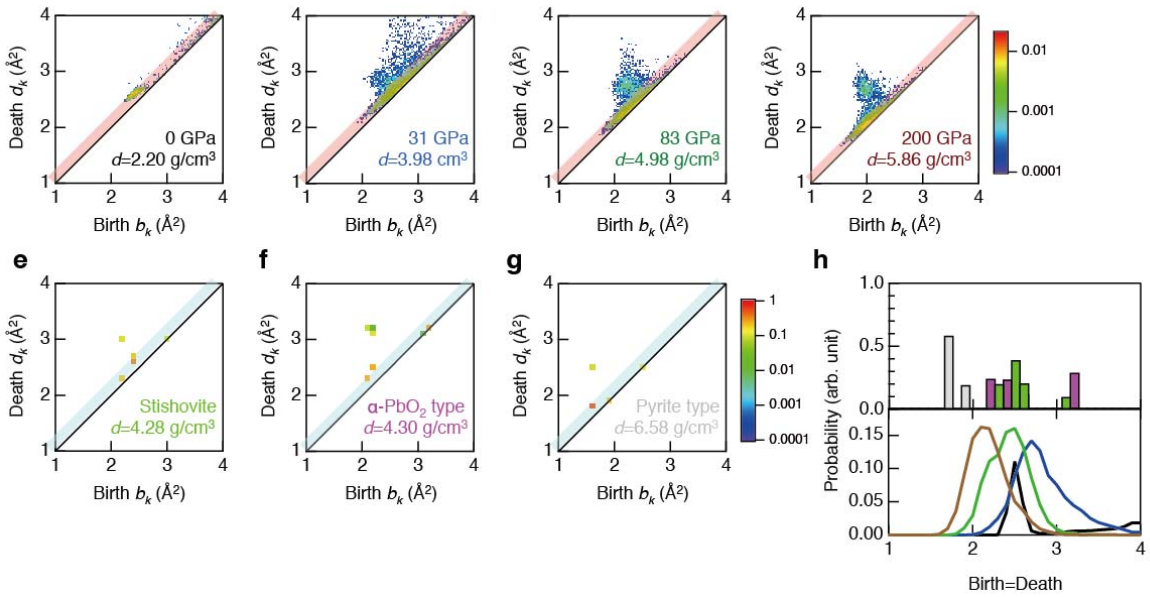

**Fig. 7. Electronic structure of silica glass under high pressure.** The electronic density of states (DOS) of the $SiO_2$ glass with projections onto O and Si up to 200 GPa.

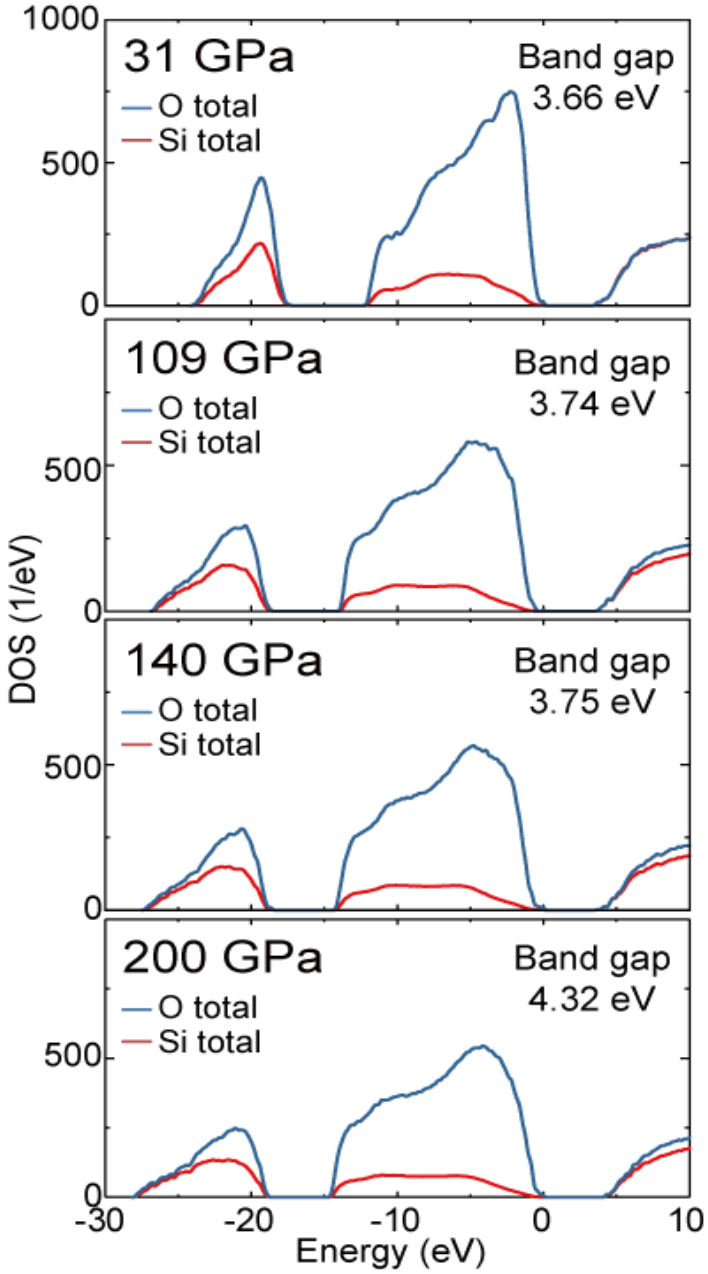

**Fig. 8 | Local structures of pyrite-type crystalline $SiO_2$ and $SiO_2$ glass (at 200 GPa) extracted from persistent diagram.** (**a**) $SiO_x$ polyhedra extracted from Si-centric persistent homology for the topological dimensionality of 1. (b) $OSi_y$ clusters extracted from Si-centric persistent homology for the topological dimensionality of 2.